On the Plane Wave-Excited Subwavelength Circular Aperture in a Thin Perfectly Conducting Flat Screen

Krzysztof A. Michalski, *Fellow, IEEE*, and Juan R. Mosig, *Fellow, IEEE*

***Abstract*—The electromagnetic field transmitted by a subwavelength circular aperture in a perfectly conducting screen of infinitesimal thickness and illuminated by an obliquely incident plane wave is analyzed based on the Bethe–Bouwkamp quasi-static model of the field in the aperture plane. The problem is formulated in the spectral domain and the solution is expressed in terms of a minimum number of one-dimensional Hankel-transform integrals involving products of Bessel functions and spherical Bessel functions. An efficient computational scheme for these integrals is implemented, based on numerical quadrature with convergence acceleration by extrapolation. From the rigorous spectral domain formulation, closed form expressions are also derived for the transmitted near-zone and far-zone fields. Sample numerical results are presented to demonstrate the validity of the method and its utility in the modeling of aperture-type near-field optical probes.**

***Index Terms*—Bethe–Bouwkamp model, near-field optical probe, spectral domain method, subwavelength aperture.**

Dedicated to the memory of Professor Robert E. Collin

I. Introduction

THE problem of light transmission through a subwavelength circular aperture in a metallic screen has enjoyed a renewed interest in the context of near-field scanning optical microscopy (NSOM) [1]–[4]. The first solution—assuming a perfectly conducting screen of infinitesimal thickness and an aperture of radius $a \ll \lambda$, where λ is the wavelength—was put forward by Bethe [5], who derived a quasi-static expression for the equivalent magnetic current of the aperture. Bethe's original formulation was incomplete and was subsequently corrected by Bouwkamp [6]–[8] and later by Rahmat–Samii and Mittra [9] using a different approach. From the known aperture field distribution (or the equivalent magnetic current), the transmitted field can be determined by means of the classical vector and scalar potentials [10]—a problem that can be formulated in either the space domain or in the Fourier spectrum domain.

Manuscript received October 25, 2013; revised December 14, 2013; accepted January 16, 2014. Date of publication January 27, 2014; date of current version April 03, 2014. This work was supported in part by the Ecole Polytechnique Fédérale de Lausanne (EPFL), Lausanne, Switzerland.

K. A. Michalski is with the Department of Electrical and Computer Engineering, Texas A&M University, College Station, TX 77843-3128 USA (e-mail: krys@ece.tamu.edu).

J. R. Mosig is with the Laboratory of Electromagnetics and Acoustics, Ecole Polytechnique Fédérale de Lausanne, CH-1015 Lausanne, Switzerland (e-mail: juan.mosig@epfl.ch).

Color versions of one or more of the figures in this paper are available online at http://ieeexplore.ieee.org.

Digital Object Identifier 10.1109/TAP.2014.2302839

The first numerical studies of the transmitted field distribution based on the Bethe–Bouwkamp (BB) model were by Leviatan [11], Dürig *et al.* [12], and Nakano and Kawata [13], who all used the space domain approach. Only Nakano and Kawata considered the off-normal (oblique) incidence, but they (as well as Dürig *et al.*) used the original Bethe magnetic current, which differs from the correct Bouwkamp's expression by a solenoidal vector [14] and thus can only be used to compute far-zone fields. Subsequently, Van Labeke *et al.* [15], [16] treated this problem by the spectral domain method, which is particularly attractive in the NSOM context, because a planar layered sample can readily be included in the analysis [17]. The approach initially used by Van Labeke *et al.* relied on the Cartesian Fourier transforms and was superseded by the method of Grober *et al.* [18], who employed cylindrical coordinates and expressed the fields in terms of one-dimensional Hankel-transform integrals. The original Grober *et al.* expression for the spectral source of the transverse-magnetic (TM) partial field is approximate, but an exact formula was later derived by Michalski [19]. In these spectral domain studies, a normally-incident plane wave was assumed. The off-normal incidence case, which is considerably more complex (even considered "numerically intractable" by some authors [3]), was only recently studied by Michalski [20], who used an approximate complex-image method to compute the Hankel-transform integrals.

In this paper, a rigorous spectral domain approach is presented to determine the electromagnetic field transmitted by a subwavelength circular aperture in a planar conducting screen of infinitesimal thickness under oblique plane-wave incidence, assuming the quasi-static BB aperture model. The fields are expressed in terms of a minimum number of Hankel-transform integrals, which are then computed by an efficient numerical procedure based on numerical quadrature with convergence acceleration by extrapolation. Using the spectral domain formulation as the point of departure, closed-form expressions are also derived for the fields near the aperture, as well as for the distant fields. The validity and utility of the method is demonstrated by sample numerical results. Our study is motivated by the quest for a better understanding of the electromagnetic field in the vicinity of aperture-type near-field optical probes.

II. Statement of the Problem

The incident field geometry and the coordinate system employed are illustrated in Fig. 1. The screen resides in a medium characterized by the wavenumber $k = \omega\sqrt{\varepsilon\mu} = 2\pi/\lambda$ and intrinsic impedance $\eta = \sqrt{\mu/\varepsilon}$, where μ and ε are the permeability and permittivity, respectively. Assuming the $e^{j\omega t}$ time

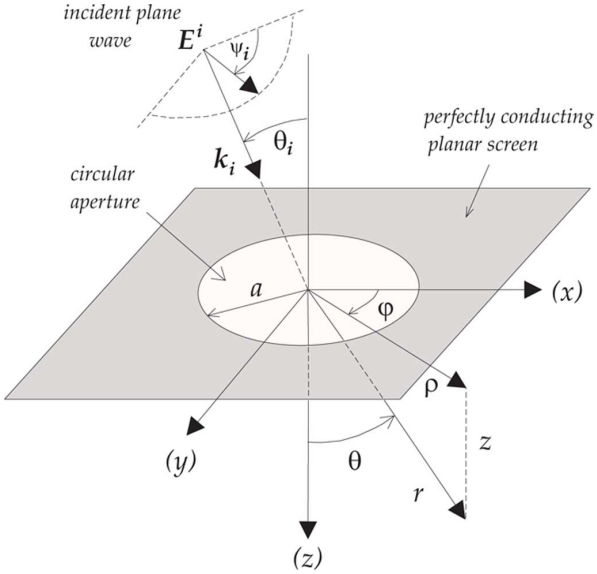

Fig. 1. Diagram of a plane wave obliquely incident on the circular aperture of radius a in a planar screen, indicating the coordinate system used in the analysis. The plane of incidence is chosen as the x–z plane, θ_i is the angle between the z axis and the direction of incidence, and ψ_i is the angle between $\boldsymbol{E}^i$ and the x–z plane. The polarization is parallel for $\psi_i = 0°$ (TM wave) and perpendicular for $\psi_i = 90°$ (TE wave).

dependence and the Cartesian component notation, the electric and magnetic incident fields are given as

$$\boldsymbol{E}^i = (\kappa_{zi}\cos\psi_i, \sin\psi_i, -\kappa_{xi}\cos\psi_i)e^{-jk(\kappa_{xi}x+\kappa_{zi}z)} \quad (1)$$

$$\eta\boldsymbol{H}^i = (-\kappa_{zi}\sin\psi_i, \cos\psi_i, \kappa_{xi}\sin\psi_i)e^{-jk(\kappa_{xi}x+\kappa_{zi}z)} \quad (2)$$

where

$$\kappa_{xi} \equiv \frac{k_{xi}}{k} = \sin\theta_i \quad \kappa_{zi} \equiv \frac{k_{zi}}{k} = \cos\theta_i \quad (3)$$

are the normalized x and z components of the propagation vector $\boldsymbol{k}_i$.[1] We also allow inhomogeneous incident plane waves that propagate along the x axis, but are evanescent in the z direction, in which case $\kappa_{xi}^2 > 1$ and $\kappa_{zi} = -j\sqrt{\kappa_{xi}^2 - 1}$.

In view of the equivalence principle, the knowledge of the tangential electric field in the plane of the screen is sufficient to determine the transmitted electromagnetic field in the $z > 0$ half-space [21], [22]. In the equivalent problem, the aperture is shorted and a magnetic surface current $\boldsymbol{M} = \boldsymbol{E}^a \times \hat{\boldsymbol{z}}$ is placed over the circular region $\rho < a$ on the $z > 0$ side, where $\boldsymbol{E}^a$ is the aperture electric field.[2] According to the BB model, the radial and azimuthal cylindrical components of $\boldsymbol{M}$, correct up to the first order in ka, are given as [7]–[9]

$$M_\rho = \frac{4jk}{3\pi}\left[\kappa_{xi}^2\cos\psi_i\sin\varphi - 2s_i(\varphi)\right]\sqrt{a^2-\rho^2} \quad (4)$$

$$M_\varphi = \frac{2}{\pi}\kappa_{xi}\cos\psi_i\frac{\rho}{\sqrt{a^2-\rho^2}} + \frac{4jk}{3\pi}\left\{\kappa_{xi}^2\cos\psi_i\cos\varphi\frac{a^2-2\rho^2}{\sqrt{a^2-\rho^2}} - c_i(\varphi)\frac{2a^2-\rho^2}{\sqrt{a^2-\rho^2}}\right\} \quad (5)$$

[1]Throughout this paper, vectors are set in bold typeface, unit vectors are distinguished by carets and dyadics by double underlines.

[2]The negative of $\boldsymbol{M}$ should be put on the $z < 0$ side, if the reflected fields are also of interest [21].

and the corresponding magnetic surface charge density is

$$q_m = -\frac{4\mu}{\pi\eta}s_i(\varphi)\frac{\rho}{\sqrt{a^2-\rho^2}} \quad (6)$$

where we have introduced the notation

$$s_i(\varphi) = \cos\psi_i\sin\varphi - \kappa_{zi}\sin\psi_i\cos\varphi \quad (7)$$

$$c_i(\varphi) = \cos\psi_i\cos\varphi + \kappa_{zi}\sin\psi_i\sin\varphi. \quad (8)$$

Note that these expressions are much simplified in the special case of normal incidence, when $\kappa_{xi} = 0$ and $\psi_i = 0$.

The main objective of this study is to determine, using the spectral domain approach, the electric and magnetic fields everywhere in the $z > 0$ half-space, assuming that the fields in the aperture plane are represented by the BB model above.

III. Spectral Domain Analysis

In the spectral domain approach, the electric and magnetic fields due to the aperture source in the $z' = 0$ plane are found as

$$\boldsymbol{E}(\boldsymbol{r}) = \mathcal{F}^{-1}\left\{\underline{\underline{\tilde{\boldsymbol{G}}}}^{EM}(\boldsymbol{k}_\rho; z \mid 0)\cdot\tilde{\boldsymbol{M}}(\boldsymbol{k}_\rho)\right\} \quad (9)$$

$$\boldsymbol{H}(\boldsymbol{r}) = \mathcal{F}^{-1}\left\{\underline{\underline{\tilde{\boldsymbol{G}}}}^{HM}(\boldsymbol{k}_\rho; z \mid 0)\cdot\tilde{\boldsymbol{M}}(\boldsymbol{k}_\rho)\right\} \quad (10)$$

where $\underline{\underline{\tilde{\boldsymbol{G}}}}^{EM}$ and $\underline{\underline{\tilde{\boldsymbol{G}}}}^{HM}$ are the electric- and magnetic-field spectral domain dyadic Green functions and $\tilde{\boldsymbol{M}} = \mathcal{F}\{\boldsymbol{M}\}$. We use the Fourier transform pair (65)–(66) and the spectral domain coordinate system illustrated in Fig. 6. Excerpting from Michalski [23], the Green functions pertaining to transverse magnetic currents are

$$\underline{\underline{\tilde{\boldsymbol{G}}}}^{EM}(\boldsymbol{k}_\rho; z \mid z') = -\hat{\boldsymbol{u}}\hat{\boldsymbol{v}}V_v^e(k_\rho; z \mid z') + \hat{\boldsymbol{v}}\hat{\boldsymbol{u}}V_v^h(k_\rho; z \mid z') + \hat{\boldsymbol{z}}\hat{\boldsymbol{v}}\frac{\eta k_\rho}{k}I_v^e(k_\rho; z \mid z') \quad (11)$$

$$\underline{\underline{\tilde{\boldsymbol{G}}}}^{HM}(\boldsymbol{k}_\rho; z \mid z') = -\hat{\boldsymbol{u}}\hat{\boldsymbol{u}}I_v^h(k_\rho; z \mid z') - \hat{\boldsymbol{v}}\hat{\boldsymbol{v}}I_v^e(k_\rho; z \mid z') + \hat{\boldsymbol{z}}\hat{\boldsymbol{u}}\frac{k_\rho}{\eta k}V_v^h(k_\rho; z \mid z') \quad (12)$$

where V_v^p and I_v^p denote the voltage and current Green functions, respectively, of the spectral domain transmission-line (TL) analogue of the medium along the z axis, with the superscripts $p = \{e, h\}$ referring to the $\{\mathrm{TM}, \mathrm{TE}\}$ partial fields, respectively. These TL Green functions satisfy the coupled equations

$$\frac{dV_v^p}{dz} = -jk_z Z^p I_v^p + \delta(z - z') \qquad \frac{dI_v^p}{dz} = -jk_z Y^p V_v^p \quad (13)$$

where δ is the Dirac delta and

$$k_z = \sqrt{k^2 - k_\rho^2}, \quad -\pi < \arg k_z \le 0 \quad (14)$$

$$Z^e = \eta\frac{k_z}{k} \quad Z^h = \eta\frac{k}{k_z} \quad Y^p = \frac{1}{Z^p}. \quad (15)$$

The TL analogue for the aperture problem is illustrated in Fig. 2, where k_z and Z^p are the propagation constant and characteristic impedance, respectively. Here, the voltage source represents the transverse magnetic current and the short circuit corresponds to the perfect-conductor screen.

The spectral domain surface magnetic current $\tilde{\boldsymbol{M}}$ is found by applying the Fourier transform to (4)–(5). Upon using the

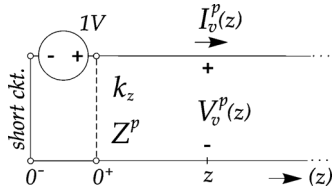

Fig. 2. Spectral domain transmission-line analogue.

identity (68) and tables of integrals [24], we find the radial and azimuthal cylindrical components of $\tilde{\boldsymbol{M}}$ as

$$\tilde{M}_u = -\frac{8jka^3}{3} s_i(\xi) F_1(k_\rho a) \tag{16}$$

$$\tilde{M}_v = \frac{4ja^3}{3}\kappa_{xi}\cos\psi_i k_\rho F_1(k_\rho a) + \frac{8jka^3}{3}\left\{\kappa_{xi}^2\cos\psi_i\cos\xi F_2(k_\rho a) - c_i(\xi)F_0(k_\rho a)\right\} \tag{17}$$

where we have introduced the *aperture source functions*

$$F_0(k_\rho a) = j_0(k_\rho a) \qquad F_1(k_\rho a) = 3\frac{j_1(k_\rho a)}{k_\rho a} \tag{18}$$

as well as their difference

$$F_2(k_\rho a) \equiv F_1(k_\rho a) - F_0(k_\rho a) = j_2(k_\rho a) \tag{19}$$

where j_n is the spherical Bessel function of order n [25]. We next substitute (16)–(17) and (11)–(12) into (9)–(10) and perform the inverse Fourier transformation (66) using the cylindrical spectral domain coordinates (k_ρ, ξ) of Fig. 6. The ξ-integrals are then evaluated in closed form by means of the identity (68) and the remaining k_ρ-integrals are Hankel transforms, which will be denoted as

$$\mathcal{S}_n\{\cdot\} \equiv \int_0^\infty dk_\rho k_\rho J_n(k_\rho\rho)\{\cdot\}. \tag{20}$$

As a result, the Cartesian field components may be expressed as

$$\begin{aligned} E_x = &-\frac{2a^3}{3\pi}\kappa_{xi}\cos\psi_i\cos\varphi\mathcal{S}_1\{k_\rho F_1 V^e\} \\ &+\frac{2jka^3}{3\pi}\left[\kappa_{xi}^2\cos\psi_i\left(\cos 2\varphi\mathcal{S}_2\{F_2V^e\}\right.\right. \\ &\left.-\mathcal{S}_0\{F_2V^e\}\right) \\ &+\cos\psi_i\left(\mathcal{S}_0\{F_1V^h\}+\mathcal{S}_0\{F_0V^e\}\right) \\ &\left.+c_i(2\varphi)\left(\mathcal{S}_2\{F_1V^h\}-\mathcal{S}_2\{F_0V^e\}\right)\right] \end{aligned} \tag{21}$$

$$\begin{aligned} E_y = &-\frac{2a^3}{3\pi}\kappa_{xi}\cos\psi_i\sin\varphi\mathcal{S}_1\{k_\rho F_1 V^e\} \\ &+\frac{2jka^3}{3\pi}\left[\kappa_{xi}^2\cos\psi_i\sin 2\varphi\mathcal{S}_2\{F_2V^e\}\right. \\ &+\kappa_{zi}\sin\psi_i\left(\mathcal{S}_0\{F_1V^h\}+\mathcal{S}_0\{F_0V^e\}\right) \\ &\left.+s_i(2\varphi)\left(\mathcal{S}_2\{F_1V^h\}-\mathcal{S}_2\{F_0V^e\}\right)\right] \end{aligned} \tag{22}$$

$$\begin{aligned} E_z = &\frac{2j\eta a^3}{3\pi k}\kappa_{xi}\cos\psi_i\mathcal{S}_0\left\{k_\rho^2F_1I^e\right\} \\ &+\frac{4\eta a^3}{3\pi}\left[\kappa_{xi}^2\cos\psi_i\cos\varphi\mathcal{S}_1\{k_\rho F_2 I^e\}\right. \\ &\left.-c_i(\varphi)\mathcal{S}_1\{k_\rho F_0 I^e\}\right] \end{aligned} \tag{23}$$

$$\begin{aligned} H_x = &\frac{2a^3}{3\pi}\kappa_{xi}\cos\psi_i\sin\varphi\mathcal{S}_1\{k_\rho F_1 I^e\} \\ &-\frac{2jka^3}{3\pi}\left[\kappa_{xi}^2\cos\psi_i\sin 2\varphi\mathcal{S}_2\{F_2I^e\}\right. \\ &+\kappa_{zi}\sin\psi_i\left(\mathcal{S}_0\{F_1I^h\}+\mathcal{S}_0\{F_0I^e\}\right) \\ &\left.+s_i(2\varphi)\left(\mathcal{S}_2\{F_1I^h\}-\mathcal{S}_2\{F_0I^e\}\right)\right] \end{aligned} \tag{24}$$

$$\begin{aligned} H_y = &-\frac{2a^3}{3\pi}\kappa_{xi}\cos\psi_i\cos\varphi\mathcal{S}_1\{k_\rho F_1 I^e\} \\ &+\frac{2jka^3}{3\pi}\left[\kappa_{xi}^2\cos\psi_i\left(\cos 2\varphi\mathcal{S}_2\{F_2I^e\}\right.\right. \\ &\left.-\mathcal{S}_0\{F_2I^e\}\right) \\ &+\cos\psi_i\left(\mathcal{S}_0\{F_1I^h\}+\mathcal{S}_0\{F_0I^e\}\right) \\ &\left.+c_i(2\varphi)\left(\mathcal{S}_2\{F_1I^h\}-\mathcal{S}_2\{F_0I^e\}\right)\right] \end{aligned} \tag{25}$$

$$H_z = -\frac{4a^3}{3\pi\eta}s_i(\varphi)\mathcal{S}_1\{k_\rho F_1 V^h\} \tag{26}$$

where we have omitted the function arguments for notational simplicity. In the general case, 10 distinct Hankel-transform integrals appear in the electric field expressions and eight more are needed to compute the magnetic field. For normal incidence, these numbers reduce to five and five, respectively.

The above formulation is quite general and may be used, for example, in the case where the aperture probe illuminates a layered sample, since closed-form TL Green functions for multilayer media are readily available [23]. In the homogeneous medium case, the TL Green functions take the particularly simple form

$$V_v^p(k_\rho; z \mid 0) = e^{-jk_z z} \qquad I_v^p(k_\rho; z \mid 0) = Y^p e^{-jk_z z} \tag{27}$$

and the above formulas may be expressed as

$$\begin{aligned} E_x = &\frac{2j(ka)^3}{3\pi}\left\{j\kappa_{xi}\cos\psi_i\cos\varphi\mathcal{H}_1\right. \\ &+\cos\psi_i\left[(1-\kappa_{xi}^2)\mathcal{H}_2+(1+\kappa_{xi}^2)\mathcal{H}_3\right] \\ &\left.+\left[(1+\kappa_{xi}^2)\cos\psi_i\cos 2\varphi+\kappa_{zi}\sin\psi_i\sin 2\varphi\right]\mathcal{H}_4\right\} \end{aligned} \tag{28}$$

$$\begin{aligned} E_y = &\frac{2j(ka)^3}{3\pi}\left\{j\kappa_{xi}\cos\psi_i\sin\varphi\mathcal{H}_1\right. \\ &+\kappa_{zi}\sin\psi_i(\mathcal{H}_2+\mathcal{H}_3) \\ &\left.+\left[(1+\kappa_{xi}^2)\cos\psi_i\sin 2\varphi-\kappa_{zi}\sin\psi_i\cos 2\varphi\right]\mathcal{H}_4\right\} \end{aligned} \tag{29}$$

$$\begin{aligned} E_z = &\frac{4j(ka)^3}{3\pi}\left\{\frac{j}{2}\kappa_{xi}\cos\psi_i\mathcal{H}_5+\kappa_{xi}^2\cos\psi_i\cos\varphi\mathcal{H}_6\right. \\ &\left.-\left[(1+\kappa_{xi}^2)\cos\psi_i\cos\varphi+\kappa_{zi}\sin\psi_i\sin\varphi\right]\mathcal{H}_7\right\} \end{aligned} \tag{30}$$

$$\begin{aligned} H_x = &\frac{2(ka)^3}{3\pi\eta}\left\{j\kappa_{xi}\cos\psi_i\sin\varphi\mathcal{H}_6\right. \\ &+\kappa_{zi}\sin\psi_i(\mathcal{H}_8+\mathcal{H}_9-\mathcal{H}_5) \\ &-(\cos\psi_i\sin 2\varphi-\kappa_{zi}\sin\psi_i\cos 2\varphi)\mathcal{H}_{10} \\ &\left.+\left[(1+\kappa_{xi}^2)\cos\psi_i\sin 2\varphi-\kappa_{zi}\sin\psi_i\cos 2\varphi\right]\mathcal{H}_{11}\right\} \end{aligned} \tag{31}$$

$$\begin{aligned} H_y = &-\frac{2(ka)^3}{3\pi\eta}\left\{j\kappa_{xi}\cos\psi_i\cos\varphi\mathcal{H}_6-\cos\psi_i\mathcal{H}_5\right. \\ &+\cos\psi_i\left[(1-\kappa_{xi}^2)\mathcal{H}_8+\left(1+\kappa_{xi}^2\right)\mathcal{H}_9\right] \\ &-(\cos\psi_i\cos 2\varphi+\kappa_{zi}\sin\psi_i\sin 2\varphi)\mathcal{H}_{10} \\ &\left.+\left[(1+\kappa_{xi}^2)\cos\psi_i\cos 2\varphi+\kappa_{zi}\sin\psi_i\sin 2\varphi\right]\mathcal{H}_{11}\right\} \end{aligned} \tag{32}$$

$$H_z = -\frac{4(ka)^3}{3\pi\eta}(\cos\psi_i\sin\varphi-\kappa_{zi}\sin\psi_i\cos\varphi)\mathcal{H}_1 \tag{33}$$

where we have introduced the notation

$$\mathcal{H}_1 = \int_0^\infty e^{-jk_z z} J_1(k_\rho\rho) F_1(k_\rho a) \frac{k_\rho^2\, dk_\rho}{k^3} \tag{34}$$

$$\mathcal{H}_2 = \int_0^\infty e^{-jk_z z} J_0(k_\rho\rho) F_1(k_\rho a) \frac{k_\rho\, dk_\rho}{k^2} \tag{35}$$

$$\mathcal{H}_3 = \int_0^\infty e^{-jk_z z} J_0(k_\rho\rho) F_0(k_\rho a) \frac{k_\rho\, dk_\rho}{k^2} \tag{36}$$

$$\mathcal{H}_4 = \int_0^\infty e^{-jk_z z} J_2(k_\rho\rho) F_2(k_\rho a) \frac{k_\rho\, dk_\rho}{k^2} \tag{37}$$

$$\mathcal{H}_5 = \int_0^\infty \frac{e^{-jk_z z}}{jk_z} J_0(k_\rho\rho) F_1(k_\rho a) \frac{k_\rho^3\, dk_\rho}{k^3} \tag{38}$$

$$\mathcal{H}_6 = \int_0^\infty \frac{e^{-jk_z z}}{jk_z} J_1(k_\rho\rho) F_1(k_\rho a) \frac{k_\rho^2\, dk_\rho}{k^2} \tag{39}$$

$$\mathcal{H}_7 = \int_0^\infty \frac{e^{-jk_z z}}{jk_z} J_1(k_\rho\rho) F_0(k_\rho a) \frac{k_\rho^2\, dk_\rho}{k^2} \tag{40}$$

$$\mathcal{H}_8 = \int_0^\infty \frac{e^{-jk_z z}}{jk_z} J_0(k_\rho\rho) F_1(k_\rho a) \frac{k_\rho\, dk_\rho}{k} \tag{41}$$

$$\mathcal{H}_9 = \int_0^\infty \frac{e^{-jk_z z}}{jk_z} J_0(k_\rho\rho) F_0(k_\rho a) \frac{k_\rho\, dk_\rho}{k} \tag{42}$$

$$\mathcal{H}_{10} = \int_0^\infty \frac{e^{-jk_z z}}{jk_z} J_2(k_\rho\rho) F_1(k_\rho a) \frac{k_\rho^3\, dk_\rho}{k^3} \tag{43}$$

$$\mathcal{H}_{11} = \int_0^\infty \frac{e^{-jk_z z}}{jk_z} J_2(k_\rho\rho) F_2(k_\rho a) \frac{k_\rho\, dk_\rho}{k}. \tag{44}$$

Hence, we have expressed the electric and magnetic fields in terms of eleven distinct Hankel transforms, which is the minimum number possible for off-normal incidence. Seven of these integrals occur in the electric field and four more are needed to compute the magnetic field (these numbers become four and five, respectively, for normal incidence). The Hankel-transform integrals (34)–(44) comprise products of Bessel functions and spherical Bessel functions of orders 0, 1, and 2. An efficient numerical scheme for these integrals is discussed in Appendix B.

IV. Closed-Form Near-Zone Fields

The field distribution in the vicinity of the aperture is of much interest in NSOM and related applications. Bouwkamp [7] obtained closed-form expressions for the near-zone field by a "very tedious and complicated" procedure using the oblate spheroidal coordinate system. More recently, an alternative solution method was put forward by Klimov and Letokhov [26] for normal incidence only. In the present study, we derive the near-field approximation for the oblique incidence from the spectral domain representation (28)–(33). Noting that small distances in the space domain correspond to large spatial frequencies in the spectral domain, we make the replacement $jk_z \to k_\rho$ in the TL Green functions (27), which follows from (14) with $k_\rho \to \infty$. The Hankel transforms (34)–(44) may then be expressed in terms of the integrals

$$I_{mn}^q \equiv a^{q+1} \int_0^\infty k_\rho^q J_m(k_\rho\rho) j_n(k_\rho a) e^{-k_\rho z}\, dk_\rho \tag{45}$$

with the appropriate values of the indices q, m, and n, and the near-zone transmitted fields take the form

$$\begin{aligned} E_x = &-\frac{2}{\pi}\kappa_{xi}\cos\psi_i\cos\varphi I_{11}^1 \\ &+ \frac{2jka}{3\pi}\left\{\cos\psi_i\left[3(1-\kappa_{xi}^2)I_{01}^0 + (1+\kappa_{xi}^2)I_{00}^1\right]\right. \\ &\left.+\left[(1+\kappa_{xi}^2)\cos\psi_i\cos 2\varphi + \kappa_{zi}\sin\psi_i\sin 2\varphi\right] I_{22}^1\right\} \end{aligned} \tag{46}$$

$$\begin{aligned} E_y = &-\frac{2}{\pi}\kappa_{xi}\cos\psi_i\sin\varphi I_{11}^1 \\ &+ \frac{2jka}{3\pi}\left\{\kappa_{zi}\sin\psi_i\left(3I_{01}^0 + I_{00}^1\right)\right. \\ &\left.+\left[(1+\kappa_{xi}^2)\cos\psi_i\sin 2\varphi - \kappa_{zi}\sin\psi_i\cos 2\varphi\right] I_{22}^1\right\} \end{aligned} \tag{47}$$

$$\begin{aligned} E_z = &-\frac{2}{\pi}\kappa_{xi}\cos\psi_i I_{01}^1 \\ &+ \frac{4jka}{3\pi}\left\{3\kappa_{xi}^2\cos\psi_i\cos\varphi I_{11}^0\right. \\ &\left.-\left[(1+\kappa_{xi}^2)\cos\psi_i\cos\varphi + \kappa_{zi}\sin\psi_i\sin\varphi\right] I_{10}^1\right\} \end{aligned} \tag{48}$$

$$\begin{aligned} H_x = &\frac{2jka}{\pi\eta}\kappa_{xi}\cos\psi_i\sin\varphi I_{11}^0 - \frac{2}{\pi\eta}\left\{\kappa_{zi}\sin\psi_i I_{01}^1\right. \\ &\left.+(\cos\psi_i\sin 2\varphi - \kappa_{zi}\sin\psi_i\cos 2\varphi) I_{21}^1\right\} \end{aligned} \tag{49}$$

$$\begin{aligned} H_y = &-\frac{2jka}{\pi\eta}\kappa_{xi}\cos\psi_i\cos\varphi I_{11}^0 + \frac{2}{\pi\eta}\left\{\cos\psi_i I_{01}^1\right. \\ &\left.+(\cos\psi_i\cos 2\varphi + \kappa_{zi}\sin\psi_i\sin 2\varphi) I_{21}^1\right\} \end{aligned} \tag{50}$$

$$H_z = -\frac{4}{\pi\eta}(\cos\psi_i\sin\varphi - \kappa_{zi}\sin\psi_i\cos\varphi) I_{11}^1. \tag{51}$$

The required integrals I_{mn}^q are tabulated [24], [27] and can be expressed in the closed forms listed in Table I, where ξ and η are the oblate spheroidal coordinates given as[3]

$$\begin{matrix}\xi \\ \eta\end{matrix} = \sqrt{\frac{d^2 \pm (r^2 - a^2)}{2a^2}} \qquad d^2 = \sqrt{(r^2-a^2)^2 + 4a^2z^2} \tag{52}$$

with $r^2 = \rho^2 + z^2$ [28, p. 6]. Some of the formulas in Table I may also be expressed differently by means of the relations

$$\xi\eta = \frac{z}{a}, \quad (1+\xi^2)(1-\eta^2) = \left(\frac{\rho}{a}\right)^2. \tag{53}$$

In (49)–(50), we have omitted terms of second order in ka, which arise from the Hankel transforms $\mathcal{H}_8$, $\mathcal{H}_9$, and $\mathcal{H}_{11}$, and comprise the integrals I_{01}^{-1}, I_{00}^0, and I_{22}^0, respectively.[4] Our quasi-static field expressions (46)–(51) agree with those obtained by Bouwkamp [7], except that the first terms of H_x and H_y (which are of first order in ka) are missing in the Bouwkamp's results.

V. Closed-Form Far-Zone Fields

As discussed in Appendix C, the far zone field transmitted by the aperture may be viewed as originating from a magnetic dipole in the plane of the screen and an electric dipole along the screen normal, both placed at the center of the shorted aperture. These dipoles are characterized by the moments $\boldsymbol{P}_m$ and $\boldsymbol{P}_e$ given in (78) and (79), respectively. The magnetic and elec-

[3]Note that ξ and η have other meanings elsewhere in this paper. The upper and lower signs in (52) pertain to ξ and η, respectively.

[4]Closed forms are not available, except for I_{00}^0, which is listed in Table I.

TABLE I
CLOSED-FORM QUASI-STATIC HANKEL TRANSFORM INTEGRALS

qmn	Closed form of I^q_{mn}
000	$\operatorname{arccot}\xi$
001	$\eta\,(1-\xi\operatorname{arccot}\xi)$
100	$\dfrac{\eta}{\eta^2+\xi^2}$
101	$\operatorname{arccot}\xi-\dfrac{\xi}{\eta^2+\xi^2}$
110	$\left(\dfrac{\rho}{a}\right)\dfrac{\xi}{(\eta^2+\xi^2)(1+\xi^2)}$
011	$\dfrac{1}{2}\left(\dfrac{\rho}{a}\right)\left(\operatorname{arccot}\xi-\dfrac{\xi}{1+\xi^2}\right)$
111	$\left(\dfrac{\rho}{a}\right)\dfrac{\eta}{(\eta^2+\xi^2)(1+\xi^2)}$
121	$\dfrac{\xi\,(1-\eta^2)}{(\eta^2+\xi^2)(1+\xi^2)}$
122	$\dfrac{\eta\,(1-\eta^2)}{(\eta^2+\xi^2)(1+\xi^2)}$

tric surface currents associated with these dipoles, expressed in cylindrical coordinates, are

$$\boldsymbol{M}^m=-jk\frac{4a^3}{3\pi}\left[s_i(\varphi)\hat{\boldsymbol{\rho}}+c_i(\varphi)\hat{\boldsymbol{\varphi}}\right]\frac{\delta(\rho)}{\rho} \tag{54}$$

$$\boldsymbol{J}^e=-jk\frac{2a^3}{3\pi\eta}\kappa_{xi}\cos\psi_i\hat{\boldsymbol{z}}\frac{\delta(\rho)}{\rho}. \tag{55}$$

Since the electric current $\boldsymbol{J}^e$ is normal to the aperture, we replace it by the equivalent magnetic current [29]

$$\boldsymbol{M}^e=-\frac{1}{j\omega\varepsilon}\boldsymbol{\nabla}\times\boldsymbol{J}^e=-\frac{2a^3}{3\pi}\kappa_{xi}\cos\psi_i\hat{\boldsymbol{\varphi}}\frac{d}{d\rho}\frac{\delta(\rho)}{\rho} \tag{56}$$

which is tangential. Hence, both dipoles may be represented by the equivalent magnetic surface current $\boldsymbol{M}=\boldsymbol{M}^m+\boldsymbol{M}^e$, which produces, in the presence of the conducting screen, the far zone field transmitted by the aperture. The Fourier transform of this total current $\boldsymbol{M}$ yields the radial and azimuthal components as

$$\tilde{M}_u=-\frac{8jka^3}{3}s_i(\xi) \tag{57}$$

$$\tilde{M}_v=\frac{4ja^3}{3}\kappa_{xi}\cos\psi_i k_\rho-\frac{8jka^3}{3}c_i(\xi). \tag{58}$$

Upon comparing these expressions with the BB spectral current (16)–(17), we note that the latter reduces to (57)–(58) if we set $F_1=F_0=1$ and $F_2=0$. Consequently, the far zone field transmitted by the aperture may be obtained from (28)–(33), provided that we set $a=0$ in the arguments of the aperture source functions appearing in the Hankel transforms (34)–(44). We then readily find that $\mathcal{H}_4\to\mathcal{H}_{11}\to 0$ and that

$$\mathcal{H}_8\to\mathcal{H}_9\to\int_0^\infty\frac{e^{-jk_zz}}{jk_z}J_0(k_\rho\rho)\frac{k_\rho\,dk_\rho}{k}=\frac{e^{-jkr}}{kr} \tag{59}$$

which is an identity usually attributed to Sommerfeld [30]. Furthermore, the remaining Hankel transforms reduce to the derivatives of (59) with respect to z and ρ, resulting in

$$\mathcal{H}_1\to-\left(1-3\frac{1+jkr}{k^2r^2}\right)\frac{\rho ze^{-jkr}}{kr^3} \tag{60}$$

$$\mathcal{H}_2\to\mathcal{H}_3\to(1+jkr)\frac{ze^{-jkr}}{k^2r^3} \tag{61}$$

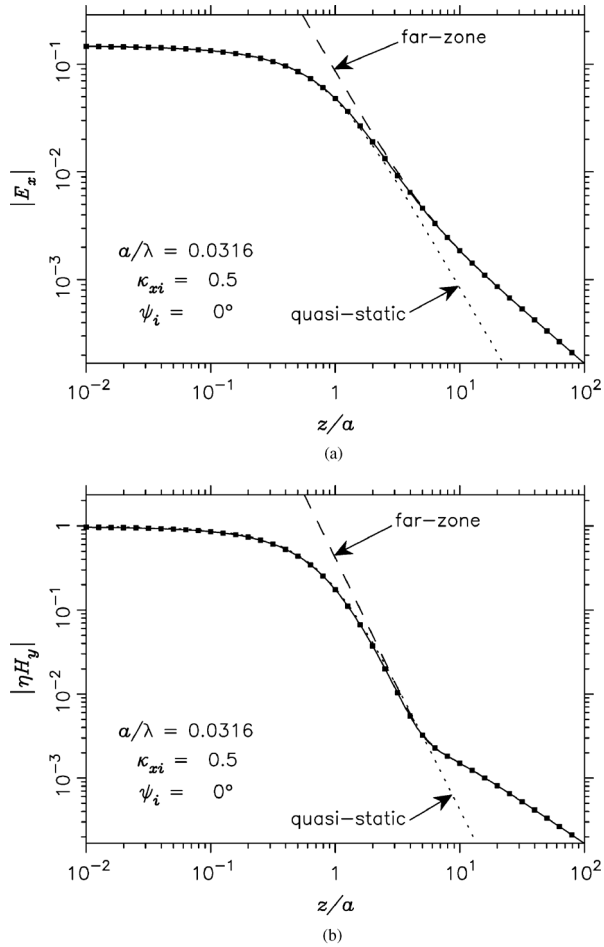

Fig. 3. Plots of $(a)\ |E_x|$ and $(b)\ |\eta H_y|$ versus. z/a on the aperture axis for $a/\lambda\approx 0.0316$ ($ka\approx 0.2$), $\kappa_{xi}=0.5$ ($\theta_i=30°$), and $\psi_i=0°$ (TM wave). The spectral domain method results (solid lines) are compared with those obtained by the space domain approach (symbols).

$$\mathcal{H}_5\to\left[2(1+jkr)+k^2\rho^2\left(1-3\frac{1+jkr}{k^2r^2}\right)\right]\frac{e^{-jkr}}{k^3r^3} \tag{62}$$

$$\mathcal{H}_6\to\mathcal{H}_7\to(1+jkr)\frac{\rho e^{-jkr}}{k^2r^3} \tag{63}$$

$$\mathcal{H}_{10}\to-\left(1-3\frac{1+jkr}{k^2r^2}\right)\frac{\rho^2e^{-jkr}}{kr^3}. \tag{64}$$

Upon substituting these limit forms for the Hankel transforms in (28)–(33), we obtain field expressions that are identical to the independently-derived far-zone expansions (74)–(75), with $\boldsymbol{P}_m$ and $\boldsymbol{P}_e$ given by (78)–(79).

VI. SAMPLE NUMERICAL RESULTS

We consider an aperture of radius $a=20$ nm, illuminated by an obliquely incident plane wave with the wavelength $\lambda=633$ nm, hence $ka\approx 0.2$. In Fig. 3, we plot the magnitude of E_x and ηH_y on the aperture axis over a four-decade range of z/a, computed by the spectral domain method presented here (solid lines) for $\kappa_{xi}=0.5$ ($\theta_i=30°$) and $\psi_i=0°$ (TM wave). We also include the corresponding curves generated by the closed-form quasi-static (dotted line) and far-zone (dashed line) formulas, derived in Sections IV and V, respectively. For comparison purposes, we have also implemented the space domain approach [22], and the obtained results are indicated by square symbols. A

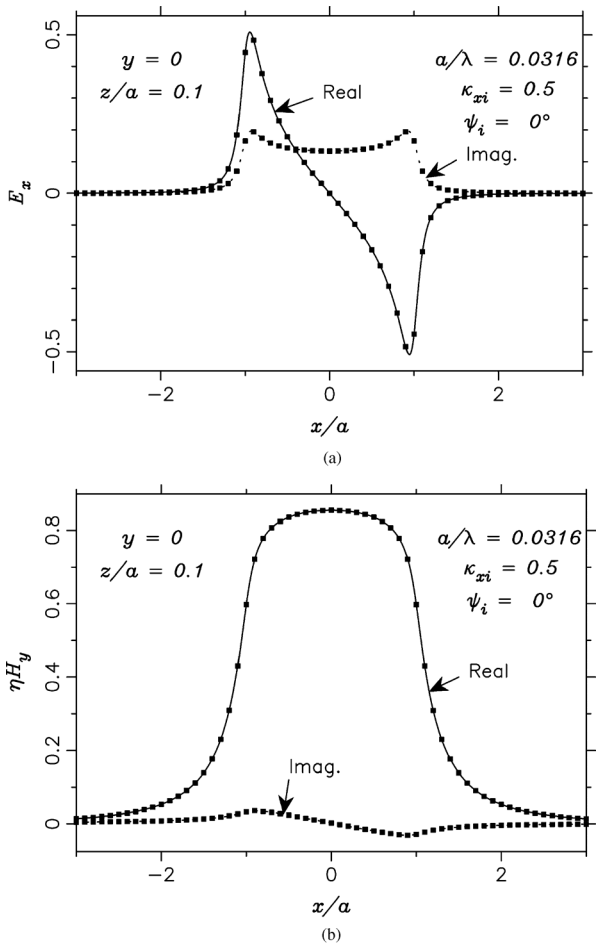

Fig. 4. Plots of (a) E_x and (b) ηH_y along the x axis at $z = a/10$. The other parameters are as in Fig. 3.

perfect agreement is observed, which was expected, as these two approaches are equivalent—albeit they lead to different solution methods, presenting different challenges.[5] Note also that the rigorous method plots follow the quasi-static curves for $z < a$ and the far-zone curves for $z > 10a$, with a smooth transition between these two ranges—similar to what was reported for normal incidence [11], [18]. For the same geometry and excitation, in Fig. 4 we compare the spectral domain and space domain results for the fields (real and imaginary parts) along the longitudinal section $y = 0$ at a fixed distance $z = a/10$ from the aperture and the screen. The peaked behavior of E_x near $x = \pm a$ is, of course, due to the singularity of the field components normal to the aperture edges. We have found that, for this small aperture, the change in the angle of incidence mostly affects the transmitted field amplitude, but has little effect on the distribution of the field, which is dominated by the edge condition. For the same aperture, in Fig. 5 we present plots of the z component of the time-averaged Poynting vector in the $z = a/10$ plane, normalized by the magnitude of the time-averaged Poynting vector of the incident field. The plots in Fig. 5(a)–(c) are for the normal incidence, oblique TM incidence $(\theta_i = 30°)$, and oblique TE incidence $(\kappa_{xi} = 50)$, respectively, where in the latter case the incident field is evanescent. It is interesting that

[5]The space domain method involves singular double integrals over the aperture region.

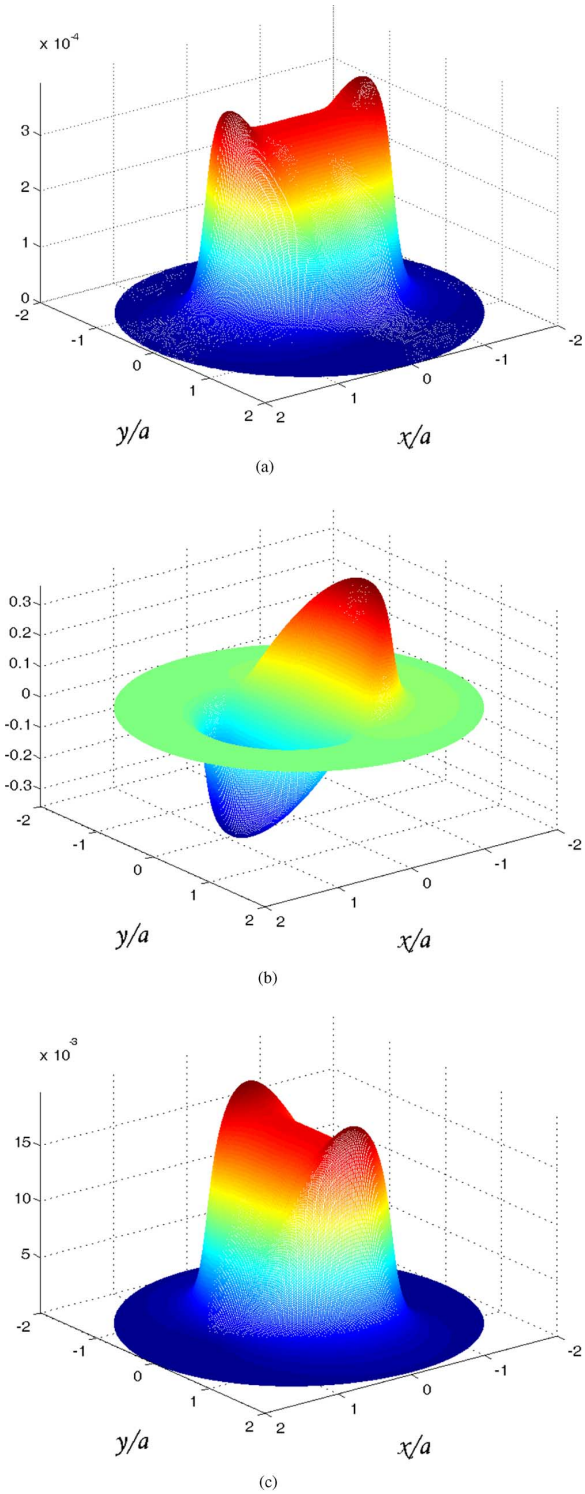

Fig. 5. Plots of the z component of the normalized time-averaged Poynting vector S_z in the $z = a/10$ plane for the aperture of Figs. 3 and 4. (a) Normal incidence. (b) Oblique TM incidence $(\psi_i = 0°, \kappa_{xi} = 0.5)$. (c) Oblique TE incidence, inhomogeneous wave $(\psi_i = 90°, \kappa_{xi} = 50)$.

in the oblique TM case there is a sign change in S_z, indicative of a circulating power flow between the two edges of the aperture—a phenomenon also reported by Nakano and Kawata [13] (based on Bethe's original magnetic current). No such circulating power flow is observed for the TE wave, whether homogeneous or evanescent. In the latter case, however, we note

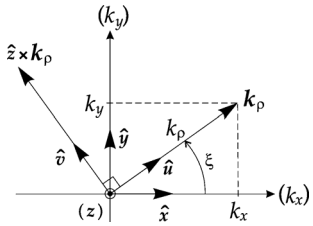

Fig. 6. Spectral domain coordinate system.

that, with $\kappa_{xi} = 50$, the transmitted power density level is approximately 50 times greater than for the normal incidence. This extraordinary transmission enhancement is consistent with the analysis of Petersson and Smith [2].

VII. Conclusion

A rigorous spectral domain formulation is presented for the problem of a plane-wave diffraction by a subwavelength circular aperture in a thin, planar, perfectly conducting screen. The analysis is based on the Bethe–Bouwkamp quasi-static aperture field model for the general case of oblique incidence. The transmitted electromagnetic fields are expressed in terms of a minimum number of one-dimensional Hankel-transform integrals, which are computed by an efficient numerical scheme. From this spectral domain representation, closed-form expressions are derived for the electric and magnetic fields in the vicinity of the aperture and in the far zone. The spectral domain formulation is comparatively simple and it may readily be extended to include the effect of a layered medium. Sample numerical results are presented that demonstrate the validity of the method and its utility in the modeling of aperture-type near-field optical probes.

Appendix A
Fourier Transform Formalism

We use the Fourier transform pair

$$\tilde{f}(\boldsymbol{k}_\rho) = \int_{-\infty}^{\infty}\int_{-\infty}^{\infty} dx\,dy e^{j\boldsymbol{k}_\rho\cdot\boldsymbol{\rho}} f(\boldsymbol{\rho}) \equiv \mathcal{F}f \tag{65}$$

$$f(\boldsymbol{\rho}) = \frac{1}{4\pi^2}\int_{-\infty}^{\infty}\int_{-\infty}^{\infty} dk_x\,dk_y e^{-j\boldsymbol{k}_\rho\cdot\boldsymbol{\rho}} \tilde{f}(\boldsymbol{k}_\rho) \equiv \mathcal{F}^{-1}\tilde{f} \tag{66}$$

where $\boldsymbol{\rho} = \hat{\boldsymbol{x}}x + \hat{\boldsymbol{y}}y$ is the radial vector of the cylindrical coordinate system and $\boldsymbol{k}_\rho = \hat{\boldsymbol{x}}k_x + \hat{\boldsymbol{y}}k_y$ its spectral domain counterpart. The spectral domain coordinate system is illustrated in Fig. 6, where the unit vectors are given as

$$\hat{\boldsymbol{u}} = \hat{\boldsymbol{x}}\cos\xi + \hat{\boldsymbol{y}}\sin\xi \qquad \hat{\boldsymbol{v}} = -\hat{\boldsymbol{x}}\sin\xi + \hat{\boldsymbol{y}}\cos\xi. \tag{67}$$

Note that $\boldsymbol{k}_\rho\cdot\boldsymbol{\rho} = k_x x + k_y y = k_\rho\rho\cos(\varphi-\xi)$.

It is often possible to perform the transforms (65)–(66) in cylindrical coordinates, such that the azimuthal integrals may be evaluated by the identity [23]

$$\frac{1}{2\pi}\int_{-\pi}^{\pi} d\varphi e^{(\pm j)\boldsymbol{k}_\rho\cdot\boldsymbol{\rho}}\begin{bmatrix}\cos n\varphi\\ \sin n\varphi\end{bmatrix} = (\pm j)^n J_n(k_\rho\rho)\begin{bmatrix}\cos n\xi\\ \sin n\xi\end{bmatrix} \tag{68}$$

where φ and ξ are interchangeable and J_n is the Bessel function of order n [25]. In such cases the two-dimensional Fourier transforms may be expressed in terms of one-dimensional Hankel transforms.

Appendix B
Computation of Hankel-Transform Integrals

The main difficulties in computing the Hankel-transform integrals (34)–(44) come from the irregular oscillatory behavior of the product of Bessel functions of integer and half-integer orders, weighted by a complex exponential. For $z > 0$, the exponential function exhibits irregular oscillations for $k_\rho \in (0, k)$ and pure decay for $k_\rho > k$, where the integrands are real for lossless media assumed here and approach their quasi-static forms (45). There is a branch point at $k_\rho = k$ and the integrands in (38)–(44) are singular there (but there are no pole singularities if the medium is homogeneous).

There appears to be a dearth of computational techniques applicable to the integrals (34)–(44) in the general case. Recently, Michalski [20] proposed an approach whereby a matrix pencil method is employed to derive complex image approximations of the aperture source functions, followed by the application of the Sommerfeld and related identities, which results in closed-form expressions of the integrals—the last step being identical to that used in Section V to derive the far-zone fields. Although this procedure offers unsurpassed efficiency, there is no *a priori* mechanism for enforcing a desired error tolerance. Therefore, in the present study we have adopted a rigorous scheme employing numerical quadrature. As the first step, we split a typical integral in (34)–(44) as

$$I = \left(\int_0^k + \int_k^b + \int_b^\infty\right) f(k_\rho; z) J_m(k_\rho\rho) j_n(k_\rho a)\,dk_\rho \tag{69}$$

so that we may write $I = I_k + I_b + I_\infty$. The first breakpoint in (69) is purposely placed at the branch point of $f(k_\rho; z)$ and the selection of the second breakpoint $b > k$ will be discussed in due course. Following Mosig [31], we compute I_k and I_b by the double-exponential (DE) tanh-sinh rule [32], [33], which can readily handle end-point singularities. The computation of the tail integral I_∞ is more challenging, and we approach it differently, depending on the relative values of ρ, a, and z. When $z > \max(\rho, a)$, the dominant effect is the exponential decay, and we employ the so-called mixed DE rule, which is effective for exponentially decaying integrands over semi-infinite range ([34], p. 176), [32]. As this rule can also handle a singularity at the lower integration limit, we apply it over the interval (k, ∞), dispensing with the second breakpoint b. When $z \le \max(\rho, a)$, the oscillatory behavior dominates, and we treat the tail by the method of Lucas [35], [36], which is based on the decomposition

$$J_m(k_\rho\rho)j_n(k_\rho a) = \mathcal{J}^+_{mn}(k_\rho;\rho,a) + \mathcal{J}^-_{mn}(k_\rho;\rho,a) \tag{70}$$

where

$$\mathcal{J}^\pm_{mn}(k_\rho;\rho,a) = 1/2\left[J_m(k_\rho\rho)j_n(k_\rho a) \mp Y_m(k_\rho\rho)y_n(k_\rho a)\right]. \tag{71}$$

Here, Y_m and y_n are the Bessel functions and spherical Bessel functions of the second kind, respectively [25]. Using (70), the tail integral may be computed as $I_\infty = I^+_\infty + I^-_\infty$, where

$$I^\pm_\infty = \int_b^\infty f(k_\rho; z)\mathcal{J}^\pm_{mn}(k_\rho;\rho,a)\,dk_\rho. \tag{72}$$

The reason behind the splitting (70)–(71) becomes obvious if we note that, for $k_\rho \gg 1$

$$\mathcal{J}^{\pm}_{mn}(k_\rho;\rho,a) \sim \mp\frac{1}{k_\rho a\sqrt{2\pi k_\rho \rho}} \cdot \cos\left[k_\rho(\rho \pm a) - (m \pm n)\pi/2 + \pi/4\right]. \quad (73)$$

Hence, provided that $\rho \neq a$, $\mathcal{J}^{\pm}_{mn}$ approach cosine functions with half-periods $q = \pi/|\rho \pm a|$. The high- and low-frequency components in the product of the Bessel functions in (69) have thus been separated and the integrals (72) are amenable to the *partition-extrapolation* (PE) method [37]–[39]. In this approach, Gaussian quadrature is applied over the consecutive intervals of length q and the resulting sequence of partial sums is accelerated by extrapolation. When $\rho = a$, $\mathcal{J}^{-}_{mn}$ ceases to be oscillatory, in which case I^{-}_{∞} is computed by the mixed rule. Following Lucas [35], we set the lower integration limit b to the larger of the first zeros of $Y_m(k_\rho\rho)$ and $y_n(k_\rho a)$, which ensures that both terms in (71) are of similar magnitude, thus preventing the loss of accuracy due to cancellation. On the aperture axis, where $\rho = 0$, only the Hankel-transform integrals $\mathcal{H}_i$ with $i = 2, 3, 5, 8$, and 9 need to be computed, and they only involve a single Bessel function $j_n(k_\rho a)$. In this case PE is applied directly to (69), with $q = \pi/a$ and b set to the first zero of $j_n(k_\rho a)$ exceeding k.

Appendix C
Equivalent Dipole Representation

The electromagnetic field far from confined sources may be represented by a multipole expansion, which is obtained by a Taylor expansion of the potentials [40], with the resulting series usually truncated after the dipole terms. In the present case, the source is the equivalent magnetic current with density $\boldsymbol{M}$, deposited on the perfect conductor screen over the shorted circular aperture region S_a. Under the assumptions that $ka \ll 1$ and $r \gg a$, where r is the radial distance in the spherical coordinate system with the origin at the aperture center (see Fig. 1), the electromagnetic field in the $z > 0$ half-space radiated by $\boldsymbol{M}$ can be expressed as [41], [42]

$$\boldsymbol{E} = \frac{e^{-jkr}}{2\pi\varepsilon}\left\{\left(\frac{1}{r^3}+\frac{jk}{r^2}\right)\left[3\hat{\boldsymbol{r}}(\hat{\boldsymbol{r}}\cdot\boldsymbol{P}_e)-\boldsymbol{P}_e\right] - \frac{k^2}{r}\left[\hat{\boldsymbol{r}}\times(\hat{\boldsymbol{r}}\times\boldsymbol{P}_e)\right] + \eta\varepsilon\left(\frac{jk}{r^2}-\frac{k^2}{r}\right)(\hat{\boldsymbol{r}}\times\boldsymbol{P}_m)\right\} \quad (74)$$

$$\boldsymbol{H} = \frac{e^{-jkr}}{2\pi}\left\{\left(\frac{1}{r^3}+\frac{jk}{r^2}\right)\left[3\hat{\boldsymbol{r}}(\hat{\boldsymbol{r}}\cdot\boldsymbol{P}_m)-\boldsymbol{P}_m\right] - \frac{k^2}{r}\left[\hat{\boldsymbol{r}}\times(\hat{\boldsymbol{r}}\times\boldsymbol{P}_m)\right] - \frac{\eta}{\mu}\left(\frac{jk}{r^2}-\frac{k^2}{r}\right)(\hat{\boldsymbol{r}}\times\boldsymbol{P}_e)\right\} \quad (75)$$

where $\boldsymbol{P}_m$ and $\boldsymbol{P}_e$ are the magnetic and electric dipole moments defined as [9], [43], [44]

$$\boldsymbol{P}_m = \frac{1}{j\omega\mu}\int_{S_a}\boldsymbol{M}\,dS = \frac{1}{\mu}\int_{S_a}\boldsymbol{\rho}q_m\,dS \quad (76)$$

$$\boldsymbol{P}_e = -\frac{\varepsilon}{2}\int_{S_a}\boldsymbol{\rho}\times\boldsymbol{M}\,dS. \quad (77)$$

With the BB model expressions (4)–(6) substituted for $\boldsymbol{M}$ and q above, the integrals may be evaluated to yield

$$\boldsymbol{P}_m = \frac{8a^3}{3\eta}(\hat{\boldsymbol{x}}\kappa_{zi}\sin\psi_i - \hat{\boldsymbol{y}}\cos\psi_i) \quad (78)$$

$$\boldsymbol{P}_e = -\frac{4\varepsilon a^3}{3}\hat{\boldsymbol{z}}\kappa_{xi}\cos\psi_i. \quad (79)$$

Therefore, the far-zone field transmitted by the aperture may be viewed as originating from a magnetic dipole in the plane of the aperture and an electric dipole along the aperture normal, both placed at the aperture center and backed by the perfect-conductor screen. Clearly, the electric dipole is only present for off-normal incidence, when $\kappa_{xi} \neq 0$.

In the radiation zone, where $kr \gg 1$, the field expressions (74)–(75) may be simplified by omitting the quasi-static and induction terms that decay faster than r^{-1}. The time-average Poynting vector is then readily found using (78)–(79) and integrated over a hemispherical surface to obtain the total time-average power radiated. The aperture transmission coefficient, defined as the ratio of this power to the time-average power density of the incident wave multiplied by the aperture area, readily follows as

$$\tau = \frac{64}{27}\frac{(ka)^4}{\pi^2}\left[(1+1/4\kappa_{xi}^2)\cos^2\psi_i + |\kappa_{zi}|^2\sin^2\psi_i\right]. \quad (80)$$

This result, which assumes a homogeneous plane wave excitation, agrees with Bethe's formulas [5]. For an inhomogeneous (evanescent along z) plane wave, this expression should be divided by $|\kappa_{xi}|$ [2]. In the latter case the transmission coefficient can be substantially greater than for a homogeneous plane wave, which points to the crucial role played by the evanescent fields in the phenomenon of extraordinary optical transmission through subwavelength apertures [1].

References

[1] T. Thio, K. M. Pellerin, R. A. Linke, and H. J. Lezec, "Enhanced light transmission through a single subwavelength aperture," *Opt. Lett.*, vol. 26, no. 24, pp. 1972–1974, 2001.

[2] L. E. R. Petersson and G. S. Smith, "Transmission of an inhomogeneous plane wave through an electrically small aperture in a perfectly conducting plane screen," *J. Opt. Soc. Am. A*, vol. 21, no. 6, pp. 975–980, 2004.

[3] S. Ducourtieux, S. Grésillon, J. C. Rivoal, C. Vannier, C. Bainier, D. Courjon, and H. Cory, "Imaging subwavelength holes in chromium films in scanning near-field optical microscopy. Comparison between experiments and calculation," *Eur. Phys. J. Appl. Phys.*, vol. 26, pp. 35–43, 2004.

[4] Y. Lin, M. H. Hong, W. J. Wang, Z. B. Wang, G. X. Chen, Q. Xie, L. S. Tan, and T. C. Chong, "Surface nanostructuring by femtosecond laser irradiation through near-field scanning optical microscopy," *Sens. Actuators A*, vol. 133, pp. 311–316, 2007.

[5] H. A. Bethe, "Theory of diffraction by small holes," *Phys. Rev.*, vol. 66, no. 7–8, pp. 163–182, Oct. 1944.

[6] C. J. Bouwkamp, "On Bethe's theory of diffraction by small holes," *Philips Res. Rep.*, vol. 5, no. 5, pp. 321–332, Oct. 1950.

[7] C. J. Bouwkamp, "Diffraction theory. A critique of some recent developments," Washington Sq. College of Arts and Science, New York, Math. Res. Group, New York Univ., Res. Rep. No. EM-50, Apr. 1953.

[8] C. J. Bouwkamp, "Diffraction theory," *Rep. Progr. Phys.*, vol. 17, pp. 35–100, 1954.

[9] Y. Rahmat-Samii and R. Mittra, "Electromagnetic coupling through small apertures in a conducting screen," *IEEE Trans. Antennas Propag.*, vol. AP-25, no. 2, pp. 180–187, Mar. 1977.

[10] R. F. Harrington, *Time-Harmonic Electromagnetic Fields*. New York, NY, USA: McGraw-Hill, 1961.

[11] Y. Leviatan, "Study of near-zone fields of a small aperture," *J. Appl. Phys.*, vol. 60, no. 5, pp. 1577–1583, 1986.
[12] U. Dürig, D. W. Pohl, and F. Rohner, "Near-field optical-scanning microscopy," *J. Appl. Phys.*, vol. 59, no. 10, pp. 3318–3327, 1986.
[13] T. Nakano and S. Kawata, "Numerical analysis of the near-field diffraction pattern of a small aperture," *J. Mod. Opt.*, vol. 39, no. 3, pp. 645–661, 1992.
[14] J. C. Simon, "Étude de la diffraction des écrans plans et application aux lentilles hertziennes," *Annales de Radioélectricité*, vol. 6, pp. 205–243, 1951.
[15] D. Van Labeke, D. Barchiesi, and F. Baida, "Optical characterization of nanosources used in scanning near-field optical microscropy," *J. Opt. Soc. Am. A*, vol. 12, no. 4, pp. 695–703, 1995.
[16] D. Van Labeke, F. Baida, D. Barchiesi, and D. Courjon, "A theoretical model for the inverse scanning tunneling optical microscope (ISTOM)," *Opt. Commun.*, vol. 114, pp. 470–480, 1995.
[17] F. I. Baida, D. Van Labeke, A. Bouhelier, T. Huser, and D. W. Pohl, "Propagation and diffraction of locally excited surface plasmons," *J. Opt. Soc. Am. A*, vol. 18, pp. 1552–1561, Jul. 2001.
[18] R. D. Grober, T. Rutherford, and T. D. Harris, "Modal approximation for the electromagnetic field of a near-field optical probe," *Appl. Opt.*, vol. 35, no. 19, pp. 3488–3494, Jul. 1996.
[19] K. A. Michalski, "Spectral domain analysis of a circular nano-aperture illuminating a planar layered sample," *Progress In Electromagn. Res. B*, vol. 28, pp. 307–323, 2011.
[20] K. A. Michalski, "Complex image method analysis of a plane wave-excited subwavelength circular aperture in a planar screen," *Progr. Electromagn. Res. B*, vol. 27, pp. 253–272, 2011.
[21] C. M. Butler, Y. Rahmat-Samii, and R. Mittra, "Electromagnetic penetration through apertures in conducting surfaces," *IEEE Trans. Antennas Propag.*, vol. AP-26, pp. 82–93, Jan. 1978.
[22] Y. Leviatan, "Low-frequency characteristic modes for aperture coupling problems," *IEEE Trans. Microw. Theory Tech.*, vol. MTT-34, pp. 1208–1213, Nov. 1986.
[23] K. A. Michalski, "Electromagnetic field computation in planar multilayers," in *Encyclopedia of RF and Microwave Engineering*, K. Chang, Ed. New York, NY, USA: Wiley-Interscience, 2005, vol. 2, pp. 1163–1190.
[24] A. P. Prudnikov, Y. A. Brychkov, and O. I. Marichev, *Integrals and Series. Volume 2: Special Functions* Transl.: from Russian by N. M. Queen. New York, NY, USA: Gordon and Breach, 1986.
[25] , M. Abramowitz and I. A. Stegun, Eds., *Handbook of Mathematical Functions*. New York, NY, USA: Dover, 1965.
[26] V. V. Klimov and V. S. Letokhov, "A simple theory of the near field in diffraction by a round aperture," *Opt. Commun.*, vol. 106, no. 4–6, pp. 151–154, 1994.
[27] I. S. Gradshteyn and I. M. Ryzhik, *Table of Integrals, Series, and Products*, A. Jeffrey and D. Zwillinger, Eds., 7th ed. New York, NY, USA: Academic, 2007.
[28] C. Flammer, *Spheroidal Wave Functions*. Mineola, NY, USA: Dover, 2005.
[29] P. E. Mayes, "The equivalence of electric and magnetic sources," *IRE Trans. Antennas Propag.*, vol. AP-6, pp. 295–296, Jul. 1958.
[30] A. Sommerfeld, *Partial Differential Equations in Physics*. New York, NY, USA: Academic, 1949.
[31] J. R. Mosig, "Weighted averages and double exponential algorithms," *IEICE Trans. Commun.*, vol. E96-B, no. 10, pp. 2355–2363, 2013, Invited Paper.
[32] H. Takahasi and M. Mori, *Double Exponential Formulas for Numerical Integration*. Kyoto, Japan: Publ. RIMS, Kyoto Univ., 1974, vol. 9, pp. 721–741.
[33] G. A. Evans, R. C. Forbes, and J. Hyslop, "The tanh transformation for singular integrals," *Int. J. Comput. Math.*, vol. 15, pp. 339–358, 1984.
[34] W. H. Press, S. A. Teukolsky, W. T. Vetterling, and B. P. Flannery, *Numerical Recipes: The Art of Scientific Computing*, 3rd ed. New York, NY, USA: Cambridge Univ. Press, 2007.
[35] S. K. Lucas, "Evaluating infinite integrals involving products of Bessel functions of arbitrary order," *J. Comput. Appl. Math.*, vol. 64, pp. 269–282, 1995.
[36] R. Golubović, A. G. Polimeridis, and J. R. Mosig, "The weighted averages method for semi-infinite range integrals involving products of Bessel functions," *IEEE. Trans. Antennas Propag.*, vol. 61, no. 11, pp. 5589–5596, Nov. 2013.
[37] S. K. Lucas and H. A. Stone, "Evaluating infinite integrals involving Bessel functions of arbitrary order," *J. Comput. Appl. Math.*, vol. 64, pp. 217–231, 1995.
[38] K. A. Michalski, "Extrapolation methods for Sommerfeld integral tails," *IEEE Trans. Antennas Propag.*, vol. 46, no. 10, pp. 1405–1418, Oct. 1998.
[39] J. R. Mosig, "The weighted averages algorithm revisited," *IEEE Trans. Antennas Propag.*, vol. 60, no. 4, pp. 2011–2018, Apr. 2012.
[40] C. H. Papas, *Theory of Electromagnetic Wave Propagation*. New York, NY, USA: McGraw-Hill, 1965.
[41] D. S. Jones, *The Theory of Electromagnetism*. Oxford, U.K.: Pergamon, 1964.
[42] C. D. Taylor, "Electromagnetic pulse penetration through small apertures," *IEEE Trans. Electromagn. Compat.*, vol. EMC-15, no. 1, pp. 17–26, Feb. 1973.
[43] R. E. Collin, "Small aperture coupling between dissimilar regions," *Electromagn.*, vol. 2, pp. 1–24, 1982.
[44] T. Wang, J. R. Mautz, and R. F. Harrington, "Characteristic modes and dipole representation of small apertures," *Radio Sci.*, vol. 7, pp. 1289–1297, Dec. 1987.

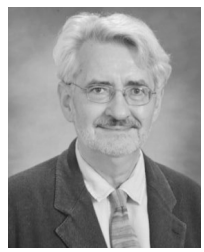

Krzysztof A. Michalski (S'78–M'81–SM'88–F'01) received the M.Sc. degree from the Wrocław Technological University, Poland, in 1974, and the Ph.D. degree from the University of Kentucky, Lexington, in 1981, both in electrical engineering.

From 1982 to 1986 he was with the University of Mississippi, and since 1987 he has been with Texas A&M University. He also has held visiting professorships with Ecole Polytechnique Fédérale de Lausanne, Texas A&M University at Qatar, Université de Nice-Sophia Antipolis, Universitat Politècnica de Catalunya, and Technische Universität München, and served as visiting scientist with Sandia National Laboratories, Albuquerque, NM, and the National Institute of Standards and Technology, Gaithersburg, MD, USA. His research interests are in electromagnetic theory and computational electromagnetics, with emphasis on Green function methods and layered media.

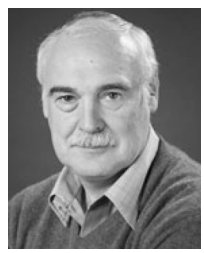

Juan R. Mosig (S'76–M'87–SM'94–F'99) was born in Cádiz, Spain. He received the Electrical Engineer degree from the Universidad Politécnica de Madrid, Madrid, Spain, in 1973, and the Ph.D. degree from the Ecole Polytechnique Fédérale de Lausanne (EPFL), Lausanne, Switzerland, in 1983.

Since 1991, he has been a Professor in the Laboratory of Electromagnetics and Acoustics (LEMA) at EPFL and its Director since 2000. He has held scientific appointments with the Rochester Institute of Technology, Rochester, NY, USA; the Syracuse University, Syracuse, NY, USA; the University of Colorado at Boulder, Boulder, CO, USA; University of Rennes, Rennes, France; University of Nice, Nice, France, the Technical University of Denmark, Lyngby, Denmark. He has authored four chapters in books on microstrip antennas and circuits and over 150 reviewed papers. He has also directly supervised more than 30 Ph.D. theses. His research interests include electromagnetic theory, numerical methods, and planar antennas.

Dr. Mosig has been the Swiss Delegate for European COST Antenna Actions since 1985 and the Chair for the two last Actions 284 and IC0603 ASSIST (2003–2011). From 2004 to 2007, he was Vice-Coordinator of the FP6 Network of Excellence ACE, that enabled the EuCAP Conference series. He has also served as member of the Board in the Coordination Actions ARTIC (FP6) and CARE (FP7) and Transnational Delegate in the IEEE APS AdCom. He is a founding member and Chair of the European Association on Antennas and Propagation (EurAAP) and he also chairs the EuCAP Conferences series and its Steering Committee. He also founded (2006) and conducts the series of INTELECT International Workshops on Computational Electromagnetics.